

# In-Plane Dynamics of Membranes with Immobile Inclusions

Naomi Oppenheimer\* and Haim Diamant†

Raymond & Beverly Sackler School of Chemistry, Tel Aviv University, Tel Aviv 69978, Israel

(Dated: November 12, 2018)

Cell membranes are anchored to the cytoskeleton via immobile inclusions. We investigate the effect of such anchors on the in-plane dynamics of a fluid membrane and mobile inclusions (proteins) embedded in it. The immobile particles lead to a decreased diffusion coefficient of mobile ones and suppress the correlated diffusion of particle pairs. Due to the long-range, quasi-two-dimensional nature of membrane flows, these effects become significant at a low area fraction (below one percent) of immobile inclusions.

PACS numbers: 87.16.dj 87.14.ep 47.15.gm 47.56.+r

Biomembranes are key structural and functional ingredients of any living cell. They are based on a self-assembled fluid bilayer of amphiphilic molecules (lipids), containing a high concentration of embedded proteins that perform vital biological tasks [1]. From a physical viewpoint, biomembranes represent an interesting state of matter, whose properties are intermediate between two-dimensional (2D) and three-dimensional (3D), and between fluid and solid. In the past four decades the structural properties of membranes and the dynamics of their out-of-plane fluctuations have been well characterized [2, 3]. The in-plane fluid dynamics, which is crucial, e.g., for the diffusion of membrane proteins, was first addressed by Saffman and Delbrück (SD) [4]. Their model considered the motion of a single inclusion within a viscous slab surrounded by an infinite fluid. While certain experiments were consistent with the SD predictions [5, 6], other works pointed to discrepancies [7, 8]. The SD model was extended in various directions, e.g., to treat proteins of larger size [9] and number [10], viscoelastic effects [11, 12], in-plane concentration fluctuations and phase separation [13–16], and the effect of an adjacent rigid surface [17–19]. Contrary to these models, most biomembranes are neither freely suspended in an infinite fluid nor attached to a rigid wall. Rather, they are anchored via proteins or protein-associated domains to a dilute, soft network of filaments (cortical actin in animal cells or cortical microtubules in plant cells) [1]. Our aim is to explore how the membranal in-plane response, and the consequent dynamics of mobile inclusions, are affected by such immobile anchors.

Models of membrane dynamics are divided into those that conserve momentum in 3D [4, 9–11, 13–16], as applicable to freely suspended membranes, and those that do not [17–22], as appropriate for substrate-supported membranes. This essential difference is reflected in the respective velocity Green’s functions,  $\mathbf{G}^{\text{free}}(\mathbf{r})$  and  $\mathbf{G}^{\text{sup}}(\mathbf{r})$ —tensors that give the flow velocity of the membranal fluid at position  $\mathbf{r}$ ,  $\mathbf{v}(\mathbf{r})$ , in response to a localized in-plane force,  $\mathbf{F}$ , applied at the origin,  $v_i(\mathbf{r}) = G_{ij}^{\text{free/sup}}(\mathbf{r})F_j$  (with  $i, j = x, y$  and summation over repeated indices). In Fourier space,  $\tilde{\mathbf{G}}(\mathbf{q}) = \int d^2r e^{-i\mathbf{q}\cdot\mathbf{r}} \mathbf{G}(\mathbf{r})$ , these are

[10, 18]

$$\tilde{G}_{ij}^{\text{free}} = \frac{1}{\eta_m q(q + \kappa)} \left( \delta_{ij} - \frac{q_i q_j}{q^2} \right), \quad (1)$$

$$\tilde{G}_{ij}^{\text{sup}} = \frac{1}{\eta_m (q^2 + \alpha^2)} \left( \delta_{ij} - \frac{q_i q_j}{q^2} \right), \quad (2)$$

where we have assumed a flat, incompressible membrane with 2D viscosity  $\eta_m$ . In Eq. (1)  $\kappa^{-1}$  is the SD length, the characteristic distance beyond which the free membrane exchanges momentum with the surrounding fluid [4]. In the SD model  $\kappa^{-1} = \eta_m / (2\eta_f)$ , where  $\eta_f$  is the viscosity of the outer fluid. Typical values for the membrane 2D viscosity are  $\eta_m \sim 10^{-10}$ – $10^{-9}$  Pa·s·m, yielding  $\kappa^{-1} \sim 0.1$ – $1 \mu\text{m}$ . In Eq. (2)  $\alpha^{-1}$  is the distance beyond which the supported membrane loses momentum to the substrate. (For a membrane lying a distance  $h$  from a rigid wall,  $\alpha = [\kappa / (2h)]^{1/2}$  [18].) Despite the appearance of the decay parameters  $\kappa$  and  $\alpha$ , Eqs. (1) and (2) describe long-ranged velocity responses— $\mathbf{G}^{\text{free}}$  decays as  $1/r$  and  $\mathbf{G}^{\text{sup}}$  as  $1/r^2$  (due to the conservation of 3D momentum in the former, and 2D membrane mass in the latter [23]).

Biomembranes contain anchoring inclusions separated by typical distances of 30–80 nm [1], i.e., covering an area fraction  $\phi \sim 10^{-3}$ – $10^{-2}$ . These immobile inclusions break the membrane’s translational symmetry and absorb momentum; hence, the large-distance response should be similar to  $\mathbf{G}^{\text{sup}}$ . From another perspective, we expect the immobile obstacles to serve as a porous matrix within which the lipids flow. Indeed, Eq. (2) is analogous to the response of a fluid embedded in a porous medium [23]. We establish below that this intuitive picture is correct and derive the momentum decay length as a function of the area fraction  $\phi$  of immobile inclusions. As this length decreases from arbitrarily large to smaller values upon increasing  $\phi$ , the membrane crosses over from a dominantly “free” behavior to a “supported” (or “porous”) one.

We first note the quasi-2D nature of the system. Over sufficiently small distances a membrane behaves as a momentum-conserving 2D fluid, whose velocity Green’s

function is given by [24]

$$G_{ij}^{2D}(\mathbf{r}) = \frac{1}{4\pi\eta_m} \left\{ \left[ \ln\left(\frac{2}{\beta r}\right) - \gamma - \frac{1}{2} \right] \delta_{ij} + \frac{r_i r_j}{r^2} \right\}, \quad (3)$$

where  $\beta^{-1}$  is a cutoff length regularizing the divergent 2D behavior and  $\gamma \simeq 0.577$  is Euler's constant. Both Eqs. (1) and (2), upon inversion to real space and taking the limit of small distances, coincide with  $G^{2D}$ , with  $\beta = \kappa$  or  $\beta = \alpha$ , correspondingly. In the current problem the immobile inclusions produce an effective cutoff for the membrane's 2D behavior, to be derived below. With increasing  $\phi$ ,  $\beta^{-1}$  decreases from  $\kappa^{-1}$  down to a microscopic length.

Let us consider a bare free membrane and ask how its velocity response, Eq. (1), is modified by the presence of immobile cylindrical inclusions [25]. The inclusion radius,  $a$ , is taken as the smallest length in the problem, and the calculation is restricted to the leading terms in  $\kappa a$  and  $a/r$ . We begin by applying a localized force  $\mathbf{F}$  at the origin. The resulting flow velocity of the bare membrane is  $v_i^{(0)}(\mathbf{r}) = G_{ij}^{\text{free}}(\mathbf{r})F_j$ . Next we place an immobile inclusion at position  $\mathbf{r}'$ . Due to the flow  $\mathbf{v}^{(0)}$ , the inclusion exerts an additional force on the membrane,  $\mathbf{F}^{(1)} \simeq -\Gamma \mathbf{v}^{(0)}(\mathbf{r}')$ , where

$$\Gamma = 4\pi\eta_m / \{ \ln[2/(\beta a)] - \gamma \} \quad (4)$$

is the friction coefficient of the cylindrical [25] inclusion [4, 10, 20],  $\beta$  being an effective 2D cutoff. We neglect moments of the force distribution higher than this monopole. The inclusion-induced force changes the flow velocity by  $v_i^{(1)}(\mathbf{r}) = G_{ij}^{\text{free}}(\mathbf{r} - \mathbf{r}')F_j^{(1)}(\mathbf{r}')$ . Thus, a single immobile inclusion reflects the original force as  $v_i^{(1)}(\mathbf{r}) = -\Gamma G_{ij}^{\text{free}}(\mathbf{r} - \mathbf{r}')G_{jk}^{\text{free}}(\mathbf{r}')F_k$ . Now, consider many randomly distributed immobile inclusions, covering an area fraction  $\phi$  of the membrane. To first order in  $\phi$ , their effect on the membrane's flow is  $\langle v_i^{(1)}(\mathbf{r}) \rangle = G_{ij}^{(1)}(\mathbf{r})F_j$ , with  $G_{ij}^{(1)}(\mathbf{r}) = -\Gamma[\phi/(\pi a^2)] \int d^2 r' G_{ik}^{\text{free}}(\mathbf{r} - \mathbf{r}')G_{kj}^{\text{free}}(\mathbf{r}')$ .

At a higher value of  $\phi$  many-body terms set in—the flow reflected from one inclusion is reflected again from another, and so on. We have calculated all orders of these monopolar hydrodynamic terms while continuing to assume a uniform static distribution of inclusions [26]. This yields  $v_i(\mathbf{r}) = G_{ij}^{\text{eff}}(\mathbf{r})F_j$ , with a cumbersome expression for  $\mathbf{G}^{\text{eff}}(\mathbf{r})$  [26]. In Fourier space,

$$\tilde{G}_{ij}^{\text{eff}}(\mathbf{q}) = \frac{1}{\eta_m[q(q + \kappa) + \lambda^{-2}]} \left( \delta_{ij} - \frac{q_i q_j}{q^2} \right), \quad (5)$$

$$\lambda = a[\Gamma\phi/(\pi\eta_m)]^{-1/2}. \quad (6)$$

In the limit  $r \rightarrow 0$ ,  $\mathbf{G}^{\text{eff}}$  has the expected form of  $\mathbf{G}^{2D}$  [Eq. (3)], with a cutoff  $\beta$  that satisfies

$$\ln(\beta\lambda) = \frac{\tanh^{-1}[f(\kappa\lambda/2)]}{f(\kappa\lambda/2)}, \quad f(x) = \frac{\sqrt{x^2 - 1}}{x}. \quad (7)$$

Equations (4), (6), and (7) provide a self-consistent scheme for obtaining  $\beta a$  and  $\lambda/a$  as functions of  $\phi$  and

$\kappa a$ . The decrease of  $\beta^{-1}$  and  $\lambda$  with increasing  $\phi$  is shown in Fig. 1. In the limit  $\phi \rightarrow 0$  we have  $\lambda \rightarrow \infty$  [Eq. (6)], and Eq. (7) then gives  $\beta \rightarrow \kappa$  (see Fig. 1A)—i.e., the cutoff of the 2D behavior is that of a free membrane, as expected. As  $\phi$  increases,  $\lambda$  decreases roughly as  $\phi^{-1/2}$  (Fig. 1B inset), while  $\beta^{-1}$  decreases initially as  $\phi \ln \phi$ , and subsequently more sharply (Fig. 1A). Both lengths reach values comparable to the inclusion size  $a$ , whereupon the theory breaks down. The breakdown is marked by a loss of solutions for the self-consistent scheme, occurring at a fixed (up to corrections of order  $\kappa a$ ), small area fraction,  $\phi_{\text{max}} \simeq 0.058$ . This analysis reveals two distinct regimes (cf. Fig. 1): a low-concentration regime,  $\phi \ll (\kappa a)^2 |\ln(\kappa a)|$ , in which  $\lambda \gg \beta^{-1} \simeq \kappa^{-1}$ , and a higher-concentration regime,  $(\kappa a)^2 |\ln(\kappa a)| \ll \phi < \phi_{\text{max}}$ , where  $\lambda \sim \beta^{-1} \ll \kappa^{-1}$ .

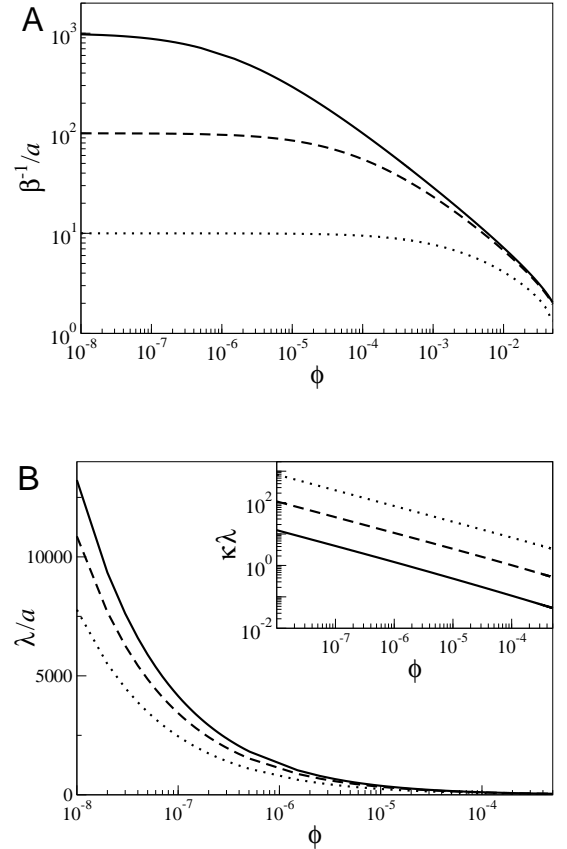


FIG. 1. Two-dimensional cutoff length (A) and momentum decay length (B) as a function of area fraction of immobile inclusions. Solid, dashed, and dotted curves correspond to  $\kappa a = 10^{-3}$ ,  $10^{-2}$ , and  $10^{-1}$ , respectively. The lengths are scaled by the inclusion size  $a$ . The inset of panel B shows  $\lambda$ , scaled by the SD length  $\kappa^{-1}$ , on a log-log plot, demonstrating a roughly  $\phi^{-1/2}$  decay.

We can readily examine the effect of  $\phi$  on the self-diffusion coefficient of a mobile inclusion of radius  $b$ . From Eq. (4) and Einstein's relation,  $D_s =$

$k_B T \{ \ln[2/(\beta b)] - \gamma \} / (4\pi\eta_m)$ , where  $k_B T$  is the thermal energy. Because of the increase of  $\beta$  with  $\phi$ ,  $D_s$  decreases from its free value  $D_s^{\text{free}}$  as given by SD [4] (the expression above with  $\beta = \kappa$ , yielding typical values of  $D_s^{\text{free}} \sim 1\text{--}10 \mu\text{m}^2/\text{s}$ ), to significantly lower values (Fig. 2).

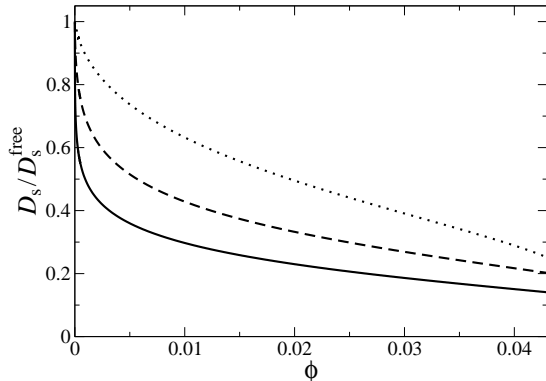


FIG. 2. Self-diffusion coefficient of a mobile inclusion as a function of area fraction of immobile inclusions. The coefficient is scaled by its value in a free membrane ( $\phi = 0$ ). The radii of the two types of inclusion are taken as equal,  $b = a$ . Solid, dashed, and dotted curves correspond to  $\kappa a = 10^{-3}$ ,  $10^{-2}$ , and  $10^{-1}$ , respectively.

Next we address the coupling diffusion coefficients of a pair of mobile inclusions separated by a distance  $r$ . The longitudinal diffusion coefficient,  $D_L(r) = \langle \Delta x_1 \Delta x_2 \rangle / (2t)$ , and the transverse one,  $D_T(r) = \langle \Delta y_1 \Delta y_2 \rangle / (2t)$ , characterize the correlated diffusion of the pair, respectively, along and perpendicular to their connecting line. Here  $\Delta x_i$  and  $\Delta y_i$  are the displacements of particle  $i$  along and perpendicular to the connecting line during time  $t$ . In the limit  $r \gg b$ , the pair diffusion coefficients are directly obtained as  $D_L(r) \simeq k_B T G_{xx}^{\text{eff}}(r\hat{\mathbf{x}})$  and  $D_T(r) \simeq k_B T G_{yy}^{\text{eff}}(r\hat{\mathbf{x}})$ , where  $\hat{\mathbf{x}}$  is a unit vector along the connecting line. As is evident from Eq. (5), the coupling diffusion coefficients in this limit depend only on  $\lambda$  and  $\kappa$ ; they are independent of the size of mobile inclusions and depend on the size of the immobile ones only indirectly, through  $\lambda$ .

The results obtained for  $D_L(r)$  and  $D_T(r)$  using the full expression for  $\mathbf{G}^{\text{eff}}(\mathbf{r})$  [26] are shown in Fig. 3 (solid lines). They include several simpler asymptotic regions. The low-concentration regime ( $\kappa\lambda \gg 1$ , Fig. 3A) includes three such regions. At short distances ( $r \ll \kappa^{-1}$ ) the behavior is 2D-like, resulting in  $D_L, D_T \sim |\ln(\beta r)|$  with  $\beta \simeq \kappa$  (dashed lines). At intermediate distances ( $\kappa^{-1} \ll r \ll \lambda$ ) the coupling becomes 3D-like, with  $D_L \sim 1/r$  and  $D_T \sim 1/r^2$  (dash-dotted lines). In these two regions the coefficients coincide with those in a free membrane, as obtained from Eq. (1) [10]. At sufficiently large interparticle distances ( $r \gg \lambda$ ) the coupling becomes sensitive to the immobile inclusions, with

$D_L, D_T \sim \pm 1/r^2$  (dotted curves in the inset). These coefficients coincide with those in a supported membrane, as obtained from Eq. (2) with  $\alpha = \lambda^{-1}$  [18]. The higher-concentration regime ( $\kappa\lambda \ll 1$ , Fig. 3B) contains two asymptotic regions. At short distances ( $r \ll \lambda$ ) the behavior is again 2D-like,  $D_L, D_T \sim |\ln(\beta r)|$ , but with  $\beta \sim \lambda^{-1} \gg \kappa$  (dashed lines). At large distances ( $r \gg \lambda$ ) we have again  $D_L, D_T \sim \pm 1/r^2$  (dotted curves) as a result of momentum loss to the immobile inclusions.

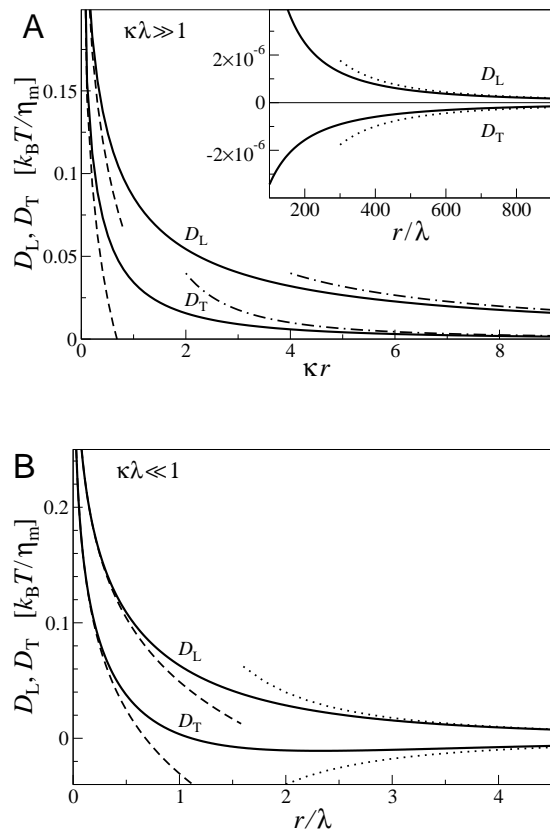


FIG. 3. Coupling diffusion coefficients of a pair of mobile inclusions as a function of mutual distance. Panels A and B present, respectively, results for low concentration ( $\kappa\lambda = 100$ ) and high concentration ( $\kappa\lambda = 0.01$ ) of immobile inclusions. Results obtained from the full Green's function (solid lines) are shown together with their various asymptotes (see text). The coupling diffusion coefficients are scaled by  $k_B T / \eta_m$ , and the distance by either the Saffman-Delbrück length  $\kappa^{-1}$  or the momentum decay length  $\lambda$ .

Our predictions concerning the effect of immobile inclusions on the self- and coupling diffusion coefficients of membrane proteins may be directly checked in particle-tracking experiments. The effective velocity Green's function derived above can be utilized [14] in other theories involving anchored membranes. We have found a strong effect of immobile inclusions already at a very low area fraction (below one percent). The effect is manifest in the hydrodynamic screening length (Fig. 1B), the self-

diffusion coefficient of a mobile inclusion (Fig. 2), and the dynamic couplings between two mobile inclusions (Fig. 3 A vs. B). The high sensitivity to the presence of immobile inclusions arises from the quasi-2D nature of the membrane and the resulting long-ranged flows. To highlight this special property, let us compare the situation to its 3D counterpart. Consider a 3D fluid containing a volume fraction  $\phi$  of immobile particles of radius  $a$ . These obstacles introduce a momentum-decay length,  $\lambda \sim a\phi^{-1/2}$ , which will strongly affect the self-diffusion coefficient of a mobile particle only when  $\lambda$  becomes comparable to the particle size—i.e., for an appreciable value of  $\phi$ . Unlike the 3D case, which is characterized by a single (small) length scale,  $a$ , the quasi-2D dynamics depends on  $a$  and another, much larger length scale,  $\beta^{-1}$ . The long-range (logarithmic) nature of 2D flows [Eq. (3)] makes this length sensitive to the immobile inclusions already for  $\phi \sim 10^{-3}$  (Fig. 1A). The quasi-2D anomaly is reflected also in the nonanalytic decrease of  $\beta^{-1}$  at small area fraction, as  $\phi \ln \phi$ .

The separation of length scales,  $\beta^{-1} \gg a$ , has also allowed us to consistently include in the effective response of the membrane all the monopolar hydrodynamic terms (i.e., all orders of  $\phi$ ) while continuing to ignore spatial correlations in the distribution of inclusions; for the low area fraction considered here ( $\phi \lesssim 10^{-2}$ ) such spatial correlations are negligible. The other assumption necessary to make this expansion valid is that the distribution of inclusions is stationary, unaffected by the exerted forces. In addition, our analysis is restricted to the leading terms in  $\kappa a$ ,  $a/r$ , and  $\beta a$ . Corrections due to higher-order terms in the first two factors are related to higher moments of the force distribution exerted by individual inclusions. In actual membranes  $\kappa a$  is of order  $10^{-3}$ , and the approximation is well justified. Higher-order terms in  $a/r$  become arbitrarily small at sufficiently large distances [27]. By contrast, since  $\beta$  is density-dependent, the restriction  $\beta a \ll 1$  limits the validity of the analysis to  $\phi \lesssim 10^{-2}$  almost irrespective of  $a$  (see Fig. 1A).

Immobile inclusions also affect the membrane's out-of-plane dynamics [28, 29]. To leading order in the normal deformations, the in-plane and out-of-plane dynamics are decoupled [11], and our quasi-2D model should remain valid within the deformed surface. At higher orders of the deformation, or because of inclusion–membrane curvature coupling, various corrections are expected [30–32].

We should mention two additional ingredients of actual biomembranes. The first is the filamentous network to which the immobile inclusions are attached. Since the network is deformable, the anchoring inclusions should not be completely immobile. Qualitatively, this restricted freedom to move laterally will affect the membrane's in-plane dynamics as if the immobile inclusions had a somewhat larger effective size. In addition, the network adds a viscoelastic response, which is important for frequency-dependent properties but vanishes for the

steady-state ones considered here. It also introduces another length scale—the network correlation length  $\ell$ —which is of order  $0.1 \mu\text{m}$  [1]. This large length scale will not significantly affect our results concerning the self-diffusion coefficient, but will influence the coupling coefficients at  $r > \ell$ . At such interparticle distances the immobile network can be replaced by an effective substrate [18]. The other ingredient is a finite density of mobile inclusions in addition to the immobile ones. Their effect can be readily incorporated by a proper renormalization of  $\eta_m$  and  $\kappa$  [10].

We have seen that for a reasonable value of  $\phi > (\kappa a)^2 |\ln(\kappa a)| \sim 10^{-5}$ , the hydrodynamic interaction between two mobile inclusions crosses over from a strong coupling [decaying only as  $\ln(1/r)$ ] for  $r < \beta^{-1}$ , to a suppressed coupling (decaying as  $1/r^2$ ) for  $r > \beta^{-1}$  (Fig. 3B). We end with the following question. If the immobile inclusions were to divide the membrane into effective domains, such that within a domain two mobile inclusions are strongly coupled, whereas across domains the coupling is suppressed, what would be the value of  $\phi$ ? Solving the equation  $a\phi^{-1/2} = \beta^{-1}$ , we find  $\phi \simeq 2 \times 10^{-3}$  and  $5 \times 10^{-5}$  for  $\kappa a = 10^{-2}$  and  $10^{-3}$ , respectively. For  $a = 5 \text{ nm}$  this corresponds to domain sizes of about  $0.1$  and  $0.7 \mu\text{m}$ . These large values stem again from the quasi-2D nature of fluid membranes.

We are grateful to Michael Kozlov for helpful discussions. This research has been supported by the Israel Science Foundation (Grants Nos. 588/06 and 8/10).

---

\* naomiopp@tau.ac.il

† hdiamant@tau.ac.il

- [1] H. Lodish *et al.*, *Molecular Cell Biology*, 6th edition (Freeman, New York, 2008).
- [2] S. A. Safran, *Statistical Thermodynamics of Surfaces, Interfaces, and Membranes* (Addison Wesley, Reading, MA, 1994).
- [3] *Structure and Dynamics of Membranes, Handbook of Biological Physics*, edited by R. Lipowsky and E. Sackmann (Elsevier, Amsterdam, 1995), Vol. 1.
- [4] P. G. Saffman and M. Delbrück, Proc. Natl. Acad. Sci. USA **72**, 3111 (1975). P. G. Saffman, J. Fluid Mech. **73**, 593 (1976).
- [5] P. Cicuta, S. L. Keller, and S. L. Veatch, J. Phys. Chem. B **111**, 3328 (2007).
- [6] S. Ramadurai, A. Holt, V. Krasnikov, G. van den Bogaart, J. A. Killian, and B. Poolman, J. Am. Chem. Soc. **131**, 12650 (2009).
- [7] Y. Gambin *et al.*, Proc. Natl. Acad. Sci. USA **103**, 2098 (2006).
- [8] A. Naji, A. J. Levine, and P. A. Pincus, Biophys. J. **93**, L49 (2007).
- [9] B. D. Hughes, B. A. Pailthorpe, and L. R. White, J. Fluid Mech. **110**, 349 (1981).
- [10] N. Oppenheimer and H. Diamant, Biophys. J. **96**, 3041 (2009).

- [11] A. J. Levine and F. C. MacKintosh, *Phys. Rev. E* **66**, 061606 (2002).
- [12] B. A. Camley and F. L. H. Brown, *Phys. Rev. E* **84**, 021904 (2011).
- [13] K. Inaura and Y. Fujitani, *J. Phys. Soc. Jpn.* **77**, 114603 (2008).
- [14] B. A. Camley and F. L. H. Brown, *Phys. Rev. Lett.* **105**, 148102 (2010).
- [15] S. Ramachandran, S. Komura, and G. Gompper, *EPL* **89**, 56001 (2010).
- [16] J. Fan, T. Han, and M. Haataja, *J. Chem. Phys.* **133**, 235101 (2010).
- [17] H. A. Stone and A. Ajdari, *J. Fluid Mech.* **369**, 151 (1998).
- [18] N. Oppenheimer and H. Diamant, *Phys. Rev. E* **82**, 041912 (2010).
- [19] S. Ramachandran, S. Komura, K. Seki, and G. Gompper, *Eur. Phys. J. E* **34**, 46 (2011).
- [20] E. Evans and E. Sackmann, *J. Fluid Mech.* **194**, 553 (1988).
- [21] Y. Y. Suzuki and T. Izuyama, *J. Phys. Soc. Jpn.* **58**, 1104 (1989). K. Seki and S. Komura, *Phys. Rev. E* **47**, 2377 (1993). S. Ramachandran, S. Komura, M. Imai, and K. Seki, *Eur. Phys. J. E* **31**, 303 (2010).
- [22] Y. Tserkovnyak and D. R. Nelson, *Proc. Natl. Acad. Sci. USA* **103**, 15002 (2006).
- [23] H. Diamant, *J. Phys. Soc. Jpn.* **78**, 041002 (2009).
- [24] C. Pozrikidis, *Boundary Integral and Singularity Methods for Linearized Viscous Flow* (Cambridge University Press, Cambridge, 1992).
- [25] The results are logarithmically insensitive to the inclusion shape, so long as it is compact. In addition, due to the large viscosity contrast between the membrane and the outer fluid, only the part of the inclusion embedded inside the membrane is important.
- [26] See EPAPS Document No. XXX for details of the calculation and the real-space expression for  $\mathbf{G}^{\text{eff}}$ .
- [27] At shorter distances we expect additional complications, such as the local membrane deformation caused by the inclusion [8], to affect our results.
- [28] N. Gov, A. G. Zilman, and S. Safran, *Phys. Rev. Lett.* **90**, 228101 (2003).
- [29] R. Zhang and F. L. H. Brown, *J. Chem. Phys.* **129**, 065101 (2008).
- [30] A. Naji and F. L. H. Brown, *J. Chem. Phys.* **126**, 235103 (2007). A. Naji, P. J. Atzberger, and F. L. H. Brown, *Phys. Rev. Lett.* **102**, 138102 (2009).
- [31] S. M. Leitenberger, E. Reister-Gottfried, and U. Seifert, *Langmuir* **24**, 1254 (2008); *Phys. Rev. E* **81**, 031903 (2010).
- [32] D. S. Dean and D. Vincent, *J. Phys. Condens. Matter* **23**, 234114 (2011).